

Determination of the Quaternary Structural States of Bovine Casein by Small-Angle X-Ray Scattering: Submicellar and Micellar Forms¹

THOMAS F. KUMOSINSKI,^{*,2} HELMUT PESSEN,^{*} HAROLD M. FARRELL, JR.,^{*}
AND HARRY BRUMBERGER[†]

^{*}*U.S. Department of Agriculture, Eastern Regional Research Center, Agricultural Regional Service, Philadelphia, Pennsylvania 19118; and* [†]*Syracuse University, Department of Chemistry, Syracuse, New York 13244-1200*

Received February 22, 1988, and in revised form July 1, 1988

Whole casein occurs in milk as a spherical colloidal complex of protein and salts called the casein micelle, with approximate average radii of 650 Å as determined by electron microscopy. Removal of Ca²⁺ is thought to result in dissociation into smaller noncolloidal protein complexes called submicelles. Hydrodynamic and light scattering studies on whole casein submicelles suggest that they are predominantly spherical particles with a hydrophobic core. To investigate whether the integrity of a hydrophobically stabilized submicellar structure is preserved in the electrostatically stabilized colloidal micellar structure, small-angle X-ray scattering (SAXS) experiments were undertaken on whole casein from bovine milk under submicellar (without Ca²⁺) and micellar (with added 10 mM CaCl₂) conditions. All SAXS results showed multiple Gaussian character and could be analyzed best by nonlinear regression in place of the customary Guinier plot. Analysis of the SAXS data for submicellar casein showed two Gaussian components which could be interpreted in terms of a particle with two concentric regions of different electron density, designated as a "compact" (subscript C) core and a "loose" (subscript L) shell, respectively. The submicelle was found to have an average molecular weight of 285,000 ± 14,600 and a mass fraction of higher electron density core, *k*, of 0.212 ± 0.028. The radius of gyration of the core, *R_C*, was 37.98 ± 0.01 Å with an electron density difference, Δ*ρ_C*, of 0.0148 ± 0.0014 e⁻/Å³, while the loose region had values of *R_L* = 88.2 ± 0.8 Å with Δ*ρ_L* = 0.0091 ± 0.0003 e⁻/Å³. Calculated distance distribution functions and normalized scattering curves also were consistent with an overall spherical particle with a concentric spherical inner core of higher electron density. These results, and in particular the remarkably low electron densities of the shells, can be interpreted in terms of a loosely packed spherical aggregate stabilized by a hydrophobic inner core and surrounded by an even more loosely packed hydrophilic region, in agreement with the results of other studies. The SAXS data for the colloidal micellar casein, which yield only cross-sectional information related to a window of scattered intensity, were analyzed by a sum of three Gaussians with no residual function. The two Gaussians with the lower values of the radius of gyration were interpreted again as an indication of an inhomogeneous spherical particle of two electron densities with the same centroid. The third Gaussian was shown to reflect the packing number of these particles, which was 3:1 for this system. The molecular weight determined from the two Gaussians of lower radii of gyration was in agreement with the value obtained from SAXS of submicellar casein, as were the *k* and Δ*ρ_C* values. However, a lower value of Δ*ρ_L* = 0.0065 ± 0.0003 was observed under these micellar conditions. These results are an indication of the existence of submicellar inhomogeneous particles containing a hydrophobically stabilized inner core within the colloidal micellar structure. © 1988 Academic Press, Inc.

tive detection system with pulse-height discrimination (Technology for Energy Corp.). Absolute intensities were obtained by means of a standard Lupolen (polyethylene) platelet sample of known scattering power as a secondary standard.⁵ A Paar sample cell with mica windows and a 1-mm path length was used for all experiments. All SAXS experiments were made at room temperature. Because of the relatively low scattering intensities shown by the samples, data for at least two samples (one for submicellar and one for micellar casein) were collected for periods in excess of 10 h to minimize the statistical error in the results. Data on all other solutions were collected for 2 to 4 h, depending on the concentration. Results of long and short collection times showed no significant differences, thus indicating no protein denaturation resulting from either sample irradiation or thermal instability.

The working equations and the notation used have been previously described (9). They apply to globular particles and to so-called "infinite slit" collimation, conditions satisfied by the instrument and the systems under examination. The equation relating the excess scattered intensity $j_n(s)$ (scattered intensity of sample, normalized with respect to the intensity of the incident beam and corrected for scattering of blank) to the scattering angle 2θ is

$$j_n(s) = j_n(0)\exp[-(4/3)\pi^2 R_a^2 s^2] + \phi(s), \quad [1]$$

where $s = (2 \sin \theta)/\lambda$; λ is the wavelength of the radiation used (1.542 Å for the K_α doublet); $j_n(0)$ is the normalized intensity extrapolated to zero angle; R_a is the apparent radius of gyration obtained by slit collimation at a finite concentration of solute; and $\phi(s)$ is a function expressing the residual between the Gaussian part of Eq. [1] and the scattering actually observed. For sufficiently small values of s (i.e., $s \leq 2.5 \times 10^{-3} \text{ \AA}^{-1}$, or $2\theta < 2^\circ$), $\phi(s)$ is usually negligible compared with the first term, which represents the Guinier approximation. R_a can therefore be obtained from the Gaussian fit to $j_n(s)$ vs s^2 for the region of very small angles. Since, however, the theoretical point-source scattering function $i_n(s)$ was needed later in any event, it was constructed from the smeared infinite-slit data $j_n(s)$ by deconvolution (10), and the concentration-dependent point-source radius of gyration was obtained in place of R_a in an analogous manner.

After evaluating $i_n(0)$ by extrapolation of $i_n(s)$ to zero angle, it was possible to calculate

$$m_{\text{app}} = i_n(0)(1 - \rho_1\psi_2)^{-2}c_e^{-1}, \quad [2]$$

$$m = m_{\text{app}} + 2Bm^2c_e, \quad [2a]$$

and

$$M = mN_A/q. \quad [2b]$$

Here m_{app} is the apparent molecular mass, expressed as electrons per molecule, at concentration c_e ; c_e is the concentration in electrons of solute per electron of solution; ρ_1 is the electron density of the solvent, calculated as 0.355 electrons/Å³; ψ_2 is the electron partial specific volume of the solute, $\psi_2 = \bar{v}/q = 2.329 \text{ \AA}^3/\text{electron}$, where \bar{v} is the partial specific volume of the protein, 0.736 ml/g (3), and q is the number of electrons per gram of particle, 0.316×10^{24} , both calculated from the average amino acid composition (11); m is the molecular mass obtained by extrapolation to zero concentration of a plot of m_{app} vs c_e ; $2B$ is the second virial coefficient; M is the weight-average molecular weight; and N_A is Avogadro's number.

With the use of these constants, further parameters were calculated (12):

$$V = i_n(0) \int_0^\infty 2\pi s j_n(s) ds, \quad [3]$$

$$\Delta\rho = \rho_2 - \rho_1 \simeq \frac{\int_0^\infty 2\pi s j_n(s) ds}{c_e(1 - \rho_1\psi_2)} + c_e\rho_1(1 - \rho_1\psi_2), \quad [4]$$

$$H = \frac{\rho_1(1 - \rho_2\psi_2)}{\Delta\rho}. \quad [5]$$

Here V is the hydrated volume; $\Delta\rho$ is the electron density difference, i.e., the difference between ρ_2 , the mean electron density of the hydrated solute, and ρ_1 , the electron density of the solvent, both in electrons per cubic angstrom; H is the degree of hydration in electrons of bound H₂O per electron of dry particle, from which the conventional degree of hydration, expressed as the number of grams of water of hydration per gram of dry protein, can be obtained by a simple conversion. Tabulated parameters were derived, in principle, from concentration-dependent parameters by extrapolation to zero concentration.

The customary Guinier analysis was not used for actual calculation of the SAXS results because of the nonlinearity of the plot for the casein micelle. Instead, all data were fitted by multiple Gaussian functions by the use of a Gauss-Newton nonlinear regression computer program developed at this laboratory.⁶ The rationale for the use of these multiple Gaussian functions will be given under Results.

Finally, in order to minimize the error in the SAXS data, the buffer samples were fitted by a function of two Gaussians with baseline (Fig. 1A). As can be seen from this figure, the resulting fit to the buffer SAXS

⁵ We are indebted to Professor O. Kratky for furnishing a calibrated Lupolen sample.

⁶ Computer assistance for these purposes was provided by the ERRC Computer Center under the direction of W. C. Damert, who originated the special algorithmic developments and programs required.

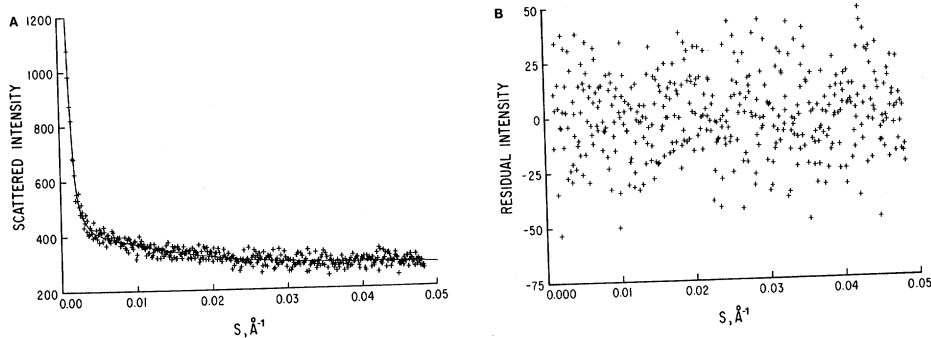


FIG. 1. Small angle X-ray scattering (SAXS) of buffer. (A) +, Raw data; solid line, best fit by nonlinear regression for a function of the sum of two Gaussians with baseline. (B) Deviation plot. +, Absolute deviation between experimental data of A and best fit by nonlinear regression, indicating random pattern.

data is excellent. Not only are the deviations very small but the deviation plot (Fig. 1B) is without pattern, showing the characteristic randomness of an appropriate fit (13). The resulting function of two Gaussians with baseline was used as a blank and subtracted from each solution SAXS curve. Since the precision of the blank was substantially greater than that of the solution measurements, and since the buffer itself has no SAXS fine structure, the blank correction could introduce no appreciable error into the excess scattered intensity values obtained.

RESULTS

Figure 2A shows a comparison of the smeared excess scattering of submicellar

and micellar casein at protein concentrations of 19.38 and 16.4 mg/ml, respectively. The lower scattering magnitude of the micellar data is probably incidental, being due to the difference in protein concentration between the two forms. However, close inspection of this figure indicates that the shapes of the two curves are qualitatively different. This difference is more striking when the SAXS results are plotted in the usual Guinier form as shown in Fig. 2B. For the submicellar data, a linear portion which can be fitted up to a value of $s = 0.00447 \text{ \AA}^{-1}$ yields a radius of gyration, R_a , of $76.0 \pm 0.6 \text{ \AA}$ by linear regression. For

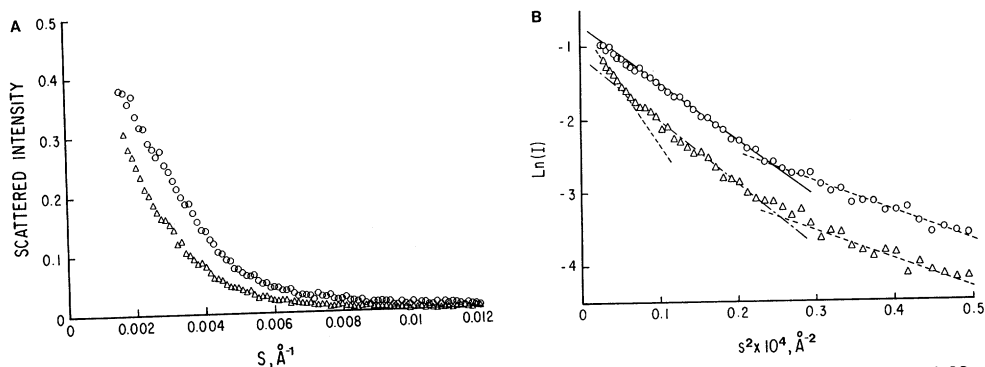


FIG. 2. SAXS of submicellar and micellar casein. (A) Absolute intensity. \circ , Submicelle at 19.38 mg/ml; Δ , micelle at 16.4 mg/ml. (B) Guinier plots. \circ , Submicelle at 19.38 mg/ml; Δ , micelle at 16.4 mg/ml; solid line, linear regression for submicelle from $s = 0.00173$ to 0.00447 \AA^{-1} ; dashed line, linear regression for micelle from $s = 0.00173$ to 0.00264 \AA^{-1} ; dot-dashed line, linear regression for micelle from $s = 0.00264$ to 0.00447 \AA^{-1} ; dotted lines, linear regressions for both submicelles and micelles beyond $s = 0.00447 \text{ \AA}^{-1}$ (these two portions are nearly parallel, indicating that the radii of gyration of the compact regions are nearly the same, consistent with the values for R_C in Table III).

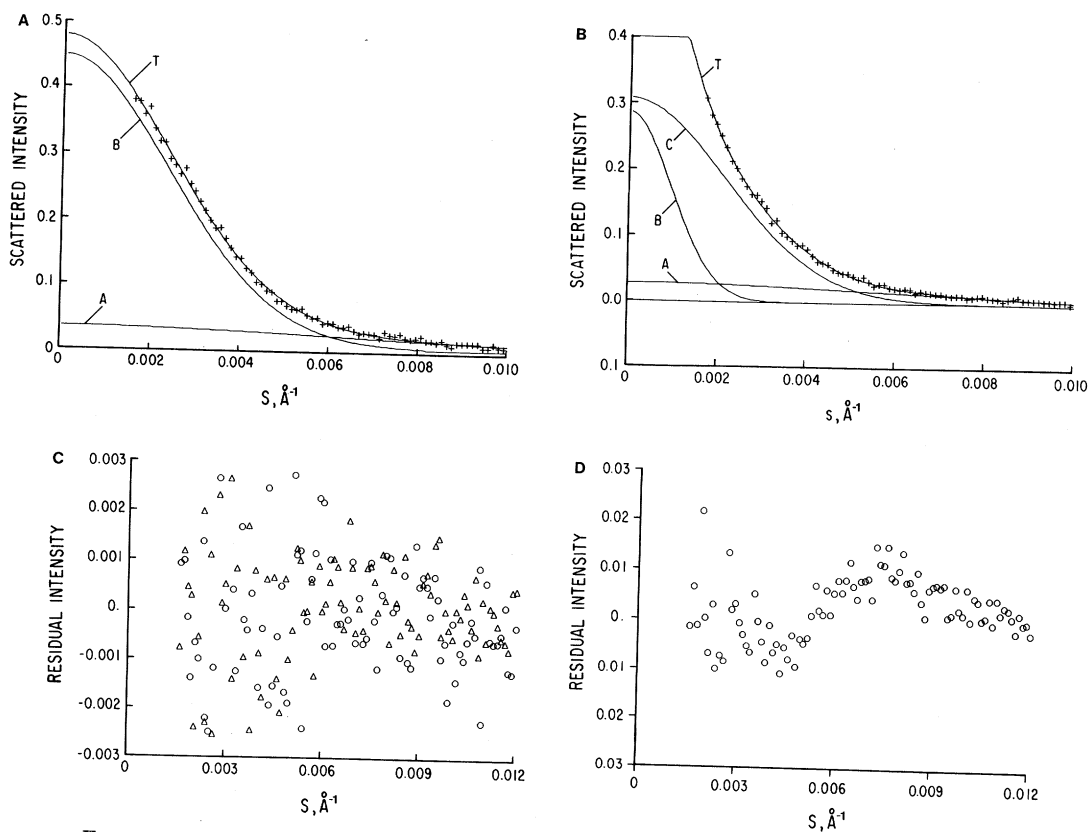


FIG. 3. (A) SAXS of submicelles. +, Smearred SAXS at 19.38 mg/ml; curve T, best fit for sum of two Gaussians by nonlinear regression; curve A, Gaussian corresponding to α and A; curve B, Gaussian corresponding to β and B. (B) SAXS of micelles. +, Smearred SAXS at 16.4 mg/ml; curve T, best fit for sum of three Gaussians by nonlinear regression; curves A and B, as above for A; curve C, Gaussian corresponding to $[I_0]_z$ (cf. Eq. [7]). (C) Deviation plot (calculated from Figs. 1A and 1B). \circ , Submicellar casein; Δ , micellar casein. (D) Deviation plot for submicelles. \circ , Best fit for one Gaussian function.

the micellar data, however, at least two linear regions appear to exist as shown by the dashed and dot-dashed lines in Fig. 2B. Linear regression for these two regions yields R_a values of 103.0 ± 1.2 and $82.4 \pm 1.4 \text{ \AA}$ for the dashed and dot-dashed lines, respectively.

For a number of reasons we opted for evaluation of the data by nonlinear regression⁶ in place of Guinier analysis. When fitting a succession of straight lines to a slightly curving Guinier plot, as above, the determination of the location of a break in the curve is a matter for which there are no good objective criteria. Furthermore, the Guinier plot, being an exponential approximation to a series expansion, in any

case begins to deviate appreciably from a straight line at scattering angles beyond the Guinier region, i.e., in our case, above $s = 2.5 \times 10^{-3} \text{ \AA}^{-1}$ (14). With nonlinear regression analysis, on the other hand, deviation plots (discussed further below) furnish a nonsubjective and very sensitive criterion of goodness of fit. In addition, this analysis affords a measure of statistical significance absent in a linearized plot, such as Guinier's, unless one undertakes the complication of an added weighting procedure. What is actually optimized in such a plot is not the fit to the excess scattering intensity but to its logarithm; this tends to deemphasize the very measurements at the smaller angles for which the

TABLE I
RESULTS OF NONLINEAR REGRESSION ANALYSIS
(Smearred SAXS)

	Submicelle (19.38 g/liter)	Micelle (16.4 g/liter)
J_1	—	0.287 ± 0.046
R_1	—	204 ± 15
B	0.439 ± 0.0068	0.307 ± 0.011
β	81.7 ± 0.9	89.96 ± 0.01
A	0.0326 ± 0.0073	0.0283 ± 0.0030
α	37.98 ± 0.004	34.7 ± 1.5
RMS	0.00218	0.00209

statistical precision is always greatest. For this reason also, the theoretical restriction to the Guinier region is not a serious limitation with nonlinear fits, since here the data at the higher angles make a much smaller contribution. In this practice, we follow a trend noticeable in other fields, where transformations leading to linear plots used to be popular before the ready access to computers and the availability of sophisticated programs made the earlier reliance on graphical solutions and linear plots no longer necessary. While such plots may still be useful for their heuristic and visual value, we find that data analysis generally benefits from nonlinear fits.

Analysis of the same data by nonlinear regression using multiple Gaussian functions was successful. The submicellar casein data could easily be fitted by a sum of two Gaussian functions, as seen in Fig. 3A. Also plotted on the same graph is the contribution of each of the two Gaussians. The micellar casein data, on the other hand, could be fitted by a sum of three Gaussians (Fig. 3B). The quality of the analysis is shown by the error in each parameter and the root-mean-square (RMS) in Table I, and also, in Fig. 3C, by the deviations between experimental data points and the fitted curve at each s value, shown for both the submicellar and micellar forms of the protein. Here, a random deviation plot is observed, with the individual deviations of the order of 1% or less. Such a random distribution has been shown by Meites (13) to be an appropriate criterion for a good fit to

data. A different situation occurs when the submicellar data are fitted by a single Gaussian. Here, the deviation plot (Fig. 3D) shows a definite pattern, which is what is observed when an incorrect function is chosen for a fit (13). Moreover, the relative values of the deviations are about an order of magnitude higher than in Fig. 3C. It may be noted that the deviation plots would contain, in addition to random errors, the residual function of Eq. [1]. However, fitting a polynomial to the deviation plots generally resulted in a straight line with zero slope and intercept, i.e., no residual function.

All submicellar casein data were fitted by a sum of two Gaussian functions, while all micellar casein data were analyzed by a sum of three Gaussian functions. The values of the fitting parameters were used to extrapolate the experimental data to zero scattering angle. (The smallest Gaussian in several instances is very broad and might be thought to make no discernible contribution. It must be considered, however, that in the absence of such a low, broad Gaussian component the original curve would require a baseline; this would be contrary to the requirement that scattered intensities must approach zero for large angles.) As noted above, the deviation plot for a single Gaussian was not random. The composite curves were then deconvoluted using the computer program developed by Lake (10); the resulting deconvoluted SAXS data for submicellar and micellar casein are shown in Fig. 4. Here, intensities for the micelles were much larger at smaller angles than those observed for the submicelles, even though the opposite was true for the smearred SAXS data (Fig. 2A). This discrepancy is primarily due to the relative large value of the parameters R and J (Table I), discussed later, of the Gaussian function which is observed in micellar but not submicellar casein.

The deconvoluted intensity at zero angle divided by its corresponding protein concentration, which yields a value proportional to the molecular weight of the particle, showed no concentration dependence under any of the conditions studied. Hence,

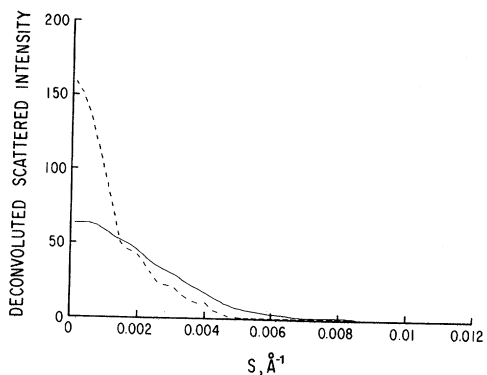


FIG. 4. Desmeared SAXS data (calculated from extrapolations in Figs. 1A and 1B using computer program developed by Lake (10)). Solid line, submicelle at 19.38 mg/ml; dashed line, micelle at 16.4 mg/ml.

the interpretation that extreme particle size polydispersity might be the cause of the multiple Gaussian character (9, 15) of the two forms of casein is unlikely. Other models accounting for the double-Gaussian character of the submicellar scattering might be based on extreme particle asymmetry (e.g., rods), or on a spherically symmetrical but inhomogeneous particle having regions of differing electron density. The former would not be in agreement with accumulating hydrodynamic, light scattering, and electron microscopic evidence, which indicates that submicellar casein exists in the form of spherical particles (1, 16). Since the particles result from a hydrophobically driven self-association of monomer units, it has been considered most likely that they contain a hydrophobic inner core surrounded by a hydrophilic outer layer (1). Such an arrangement would theoretically be the thermodynamically most stable and would be in agreement with predictions from primary structure of the caseins. It would also have different packing densities in regions of predominantly hydrophobic and hydrophilic side chains and thus would give rise to two approximately concentric regions of differing electron density ((17, 18); Fig. 5).

On the basis of these considerations, we have attempted to interpret the submicellar data by means of a model in which the particle has two regions of different elec-

tron densities with the same scattering center. In this model, the scattered amplitudes rather than the intensities of the two regions must be added because of interference effects of the scattered radiation.

Submicelles. Luzzati *et al.* (19) have developed the following equations (slightly modified here) for calculating the molecular and structural parameters of a particle having two regions of different electron density with the same electronic center of mass, when the smeared SAXS data contain two Guinier regions. The smeared scattered intensity data, $j_n(s)$, can be described by the relationship

$$j_n(s) = A \exp\left(-\frac{4\pi^2}{3} \alpha^2 s^2\right) + B \exp\left(-\frac{4\pi^2}{3} \beta^2 s^2\right) + \phi(s), \quad [6]$$

where the fitting parameters α and β correspond to the radii of gyration of the inner and outer regions, respectively, A and B to the respective zero-angle intercepts, and $\phi(s)$ is the residual function. The desmeared zero-angle scattered intensity, $[i_n(0)]_2$, and the average radius of gyration, R_2 , of the inhomogeneous particle (i.e., the whole submicelle) are obtained from

$$[i_n(0)]_2 = 2\sqrt{\pi/3}(A\alpha + B\beta) \quad [7]$$

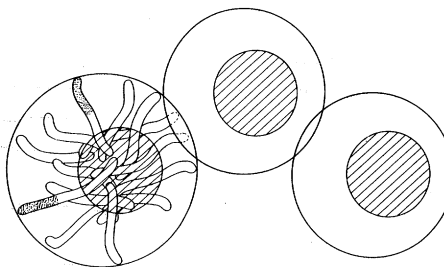


FIG. 5. Schematic representation of submicelles within micellar structure (corresponding to solid line in Fig. 8). Cross-hatched area, approximate core region of higher electron density and higher concentration of hydrophobic side chains. In lower left particle, a few representative monomer chains are indicated. Shaded areas, macropeptide portions of κ -casein.

SMALL ANGLE X-RAY SCATTERING OF BOVINE CASEIN

 TABLE II
 MOLECULAR PARAMETERS^a (DESMEARED SAXS)

Parameter	Submicelle	Micelle ^b
M	—	882,000 ± 28,000
k_2	—	0.308 ± 0.005 (3.2:1)
M_2	285,000 ± 14,600	276,000 ± 18,000
k	0.212 ± 0.028	0.216 ± 0.003
M_C	60,000 ± 5,650	56,400 ± 3,700
M_L	225,000 ± 18,500	220,000 ± 18,700
$\Delta\rho$ ($e^-/\text{\AA}^3$)	—	0.0081 ± 0.0004
$\Delta\rho_2$ ($e^-/\text{\AA}^3$)	0.0099 ± 0.0004	0.0073 ± 0.0005
$\Delta\rho_C$ ($e^-/\text{\AA}^3$)	0.0148 ± 0.0014	0.0128 ± 0.0007
$\Delta\rho_L$ ($e^-/\text{\AA}^3$)	0.0091 ± 0.0003	0.0065 ± 0.0003
H ($g_{\text{water}}/g_{\text{protein}}$)	—	7.92 ± 0.42
H_2 ($g_{\text{water}}/g_{\text{protein}}$)	6.31 ± 0.30	8.98 ± 0.44
H_C ($g_{\text{water}}/g_{\text{protein}}$)	3.97 ± 0.48	4.70 ± 0.31
H_L ($g_{\text{water}}/g_{\text{protein}}$)	6.90 ± 0.64	9.95 ± 0.58

^a Average of three concentrations (see Materials and Methods).

^b For a cautionary note in the interpretation of certain of these parameters, see Discussion.

and

$$R_2^2 = 2\sqrt{\pi/3}(A\alpha^3 + B\beta^3)[i_n(0)]^{-1}. \quad [8]$$

If subscripts C and L (following Luzzati *et al.* (19), for French “compact,” compact, and “lâche,” loose) are used to designate the higher and lower electron density regions, respectively, and subscript 2 designates the particle composed of these two regions, one has, for the respective masses,

$$M_2 = M_C + M_L \quad [9]$$

and

$$M_C = kM_2, \quad [10]$$

where k , the fraction of electrons in the higher electron density region, is easily evaluated from the relationship

$$[i(0)]_C = k^2[i(0)]_2. \quad [11]$$

Here $[i(0)]_2$ is the desmeared intensity at zero angle for the whole submicellar particle and $[i(0)]_C$ is the corresponding intensity for the higher electron density region. If it is assumed that the smeared Gaussian with the lower slope, α , in Table I, yields R_C , the radius of gyration of the denser region (a reasonable assumption since $\phi(s)$ was found to be zero for all the experiments in this study), then,

$$[i(0)]_C = 2\sqrt{\pi/3} A\alpha. \quad [12]$$

The radius of gyration of the low electron density region, R_L , can now be found from the expression

$$R_2^2 = kR_C^2 + (1 - k)R_L^2, \quad [13]$$

using equations [7]–[12]. From Eqs. [2]–[13], the molecular and structural parameters for casein under submicellar conditions were evaluated for all three concentrations of protein used in this study. Since no variation of any molecular or structural parameter with protein concentration was observed at the elevated concentrations used in this study, the averages of these results are presented in Table II for the molecular parameters and Table III for the structural parameters, subscripted as above.

Micelles. For the SAXS results of the casein micelle solutions, i.e., with the addition of 10 mM CaCl_2 , the same procedure was used for analyzing the two Gaussians having the lower radii of gyration, namely, α and β . These two Gaussians would then reflect the contribution of the submicellar structure to the SAXS results. The third Gaussian, which has the highest radius of gyration (see R_1 in Table I), would reflect

TABLE III
STRUCTURAL PARAMETERS^a (DESMEARED SAXS)

Parameter	Submicelle	Micelle
V (Å ³)	—	12,720,000 ± 250,000
V_2 (Å ³)	3,330,000 ± 260,000	4,440,000 ± 160,000
V_C (Å ³)	467,000 ± 1,520	529,000 ± 2,600
V_L (Å ³)	2,860,000 ± 400,000	3,910,000 ± 30,000
R_2 (Å)	80.24 ± 0.39	90.57 ± 0.03
R_C (Å)	37.98 ± 0.01	39.62 ± 0.01
R_L (Å)	88.22 ± 0.82	100.19 ± 0.09

^a See footnotes to Table II.

the total number of submicellar particles within the cross-sectional scattering profile. Here, at zero angle, the intensity of the larger Gaussian contribution can be simply added to the intensity of submicellar contribution. A new parameter, k_2 , the ratio of the mass of the submicelles to the total observed mass ascribable to a cross section, is defined as

$$k_2 = \frac{[i(0)]_2}{2\sqrt{\pi/3}(J1)(R1) + [i(0)]_2}, \quad [14]$$

where $J1$ and $R1$ are the intercept at zero angle and the radius of gyration of the third Gaussian in Table I, and $[i(0)]_2$ is a function of α , A , and β , B , respectively (see Table I and Eq. [7]). The inverse of k_2 may be termed the packing number, i.e., the number of submicellar particles within the observed "cross-sectional mass." The meaning of these cross-sectional parameters will be discussed below.

The scattering data for casein micelles were analyzed using the above equations for all protein concentrations. Again, no variation of SAXS-derived parameters with protein concentration was observed; the averaged values with corresponding errors are presented in the second column of Table II for the molecular parameters, and Table III for the structural parameters of the casein micelle. Here, subscripts 2 denote corresponding parameters for the submicellar particle when incorporated in an observed scattering volume of the micelle, while the unsubscripted parameters represent total cross-sectional features of the colloidal particle.

DISCUSSION

Submicelles. As shown under Results, the casein SAXS data under submicellar conditions (i.e., in the absence of calcium) were analyzed by means of a model consisting of an inhomogeneous particle of two concentric electron density regions, using as a point of departure the method of Luzzati (19). The results of this analysis for the molecular parameters are listed in Table II under the Submicelle heading.

The molecular weight of the submicellar particle, M_2 , was 285,000 ± 14,600, with no variation as a function of protein concentration used, nor was there variation in k_2 , the mass fraction of the denser or "core" region. Hence, the molecular parameters given in Table II are a measure of the limiting aggregate of the hydrophobically driven self-association of the mixed caseins in the absence of calcium. The molecular weight of this limiting polymer, M_2 , is consistent with those found in other investigations, i.e. 200,000 to 300,000, by a variety of techniques (1). In fact, the value of 285,000 is in excellent agreement with the value of 300,000 observed by small-angle neutron scattering (20).

In the latter work, the data were analyzed on the basis of a model consisting of a homogeneous limiting aggregate. In the present study, it is shown that the particle actually consists of two regions of differing electron density, with the mass fraction of the higher electron density region equal to 0.212 ± 0.028. This higher electron density region, moreover, has an electron density difference, $\Delta\rho_C$, of 0.0148 ± 0.0014 e⁻/Å³, a

hydration, H_C , of 3.97 ± 0.48 g water/g protein and a molecular weight, M_C , of $60,100 \pm 5650$ (see Table II, where the corresponding values of M_L , $\Delta\rho_L$, and H_L for the loose region are also given). The region of higher electron density most likely results from the intermolecular hydrophobically driven self-association of the casein monomer units (1), since a hydrophobic inner core would presumably be protected from interactions with water (21, 22) by a lower electron density region presumably consisting mainly of hydrophilic groups. The hydration value formally ascribed to the hydrophobic core most likely arises from the packing density of the hydrophobic side chains rather than the actual amount of water within this region. The electron density difference for the compact region of the caseins, $\Delta\rho_C$, is only $0.014 e^-/\text{\AA}^3$. This value is much lower than those observed (23) for compact globular proteins such as lysozyme, α -lactalbumin, and ribonuclease (0.078, 0.067, and $0.071 e^-/\text{\AA}^3$, respectively). Even a phosphoglycoprotein such as riboflavin-binding protein in its acid-denatured form has a $\Delta\rho$ of $0.053 e^-/\text{\AA}^3$. Thus the random nature of the casein polypeptide chain leads to an unusually low electron density in the submicelles.

The derived structural parameters for the casein submicelle are shown in Table III, where subscripts C, L, and 2 have the same meanings as before. An axial ratio for the denser region, $(a/b)_C$, of 1.06 can be calculated from V_C and R_C (19), and a value of 1.32 for the axial ratio of the total submicelle, $(a/b)_2$, from V_2 and R_2 , using as a model a prolate ellipsoid of revolution. These axial ratios of 1.06 and 1.32 for $(a/b)_C$ and $(a/b)_2$ are reasonable indications of the approximate spherical symmetry of the casein submicelle, as would be predicted from electron microscopy (1).

Before proceeding to discuss the fits of multi-Gaussian nonlinear regressions to the casein data, it may be desirable to validate this type of analysis on a well-characterized protein. One such is ribonuclease, whose crystallographic coordinates are available from the Protein Data Bank (24). From these, together with the known atomic radii (18), scattered intensities may

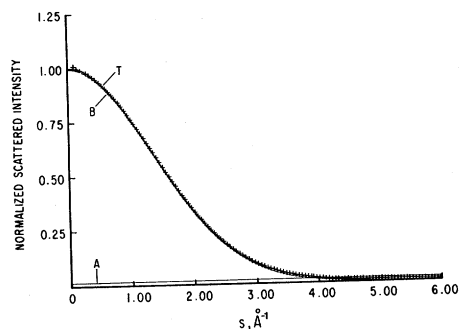


FIG. 6. Scattering curve of ribonuclease represented as the sum of two Gaussians. +, Points calculated from crystallographic coordinates and atomic radii by means of the Debye equation; curves A, B, and T, as for Fig. 3A.

be calculated by means of the Debye equation (25),

$$I(h) = \sum_{i=1}^n g_i^2 \phi_i^2(h) + 2 \sum_{i=1}^{n-1} \sum_{k=i+1}^n g_i g_k \times \phi_i(h) \phi_k(h) (\sin d_{ik}h) / (d_{ik}h), \quad [15]$$

where $h = 2\pi s$, s is as defined before, g_i is the weighting factor and $\phi_i(h)$ the shape factor of the i th sphere, and d_{ik} is the center-to-center distance between the i th and the k th spheres. Here $g_i = \rho_i (4\pi/3) R_i^3$, where ρ_i is the electron density and R_i the radius of the i th sphere, and, for a sphere, $\phi_i(h) = 3[\sin(R_i h) - R_i h \cos(R_i h)] / (R_i h)^3$. The resulting scattered intensities are shown as crosses in Fig. 6 from $s = 0$ to 0.006 \AA^{-1} . A single-Gaussian fit (not shown) has a relative RMS error of 0.6% and gives a radius of gyration of 14.28 \AA . Without implying any interpretation in terms of inhomogeneity, polydispersity, or asymmetry, it may be noted that, by contrast, a two-Gaussian fit, shown as a solid line, has a relative RMS error of less than 0.08%, yielding $\beta = 14.43 \pm 0.04 \text{ \AA}$ and $\alpha = 0.9 \pm 0.2 \text{ \AA}$. This fit is indeed considerably better than would be expected from experimental results over an angular range from 0 to 5° .

To test the assumption of a spherically shaped concentric two-electron density model for submicellar casein, the scattering intensity data were normalized to zero

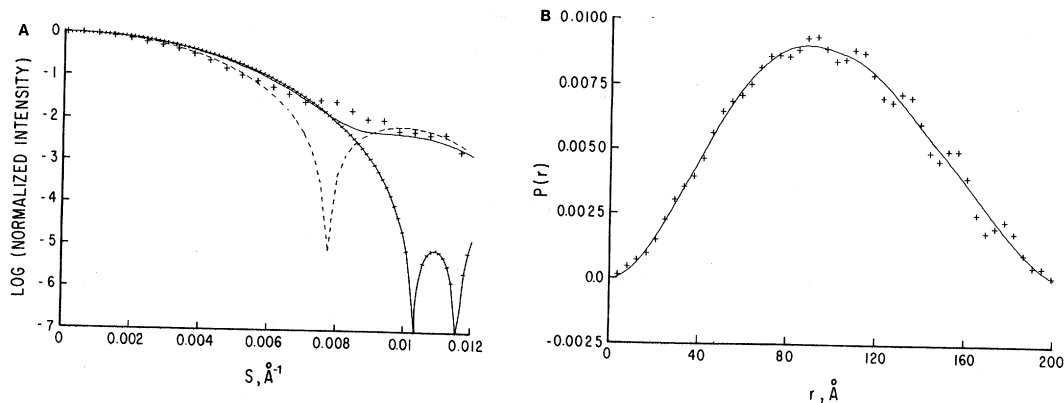


FIG. 7. (A) Normalized SAXS for submicelles. +, Normalized SAXS for submicelles at 19.38 mg/ml; solid line, theoretical for inhomogeneous sphere, i.e., two nonconcentric spheres with different radii and electron densities; dashed line, homogeneous sphere with same outer radius as solid line; ticked line, two concentric spheres with different radii and electron densities (for radii, see Discussion.) (B) Distance distribution of submicelles. +, $p(r)$ vs r for submicellar casein at 19.38 mg/ml; solid line, best fit for sum-of-three-spheres model (see Discussion).

angle and deconvoluted. Figure 7A compares the results for the highest concentration of submicellar casein (19.38 mg/ml) with various theoretical models calculated from the Debye equation. The radius of gyration of the inner region, 48 Å (calculated from V_C , Table III), and the total radius of gyration, 92.6 Å (calculated from V_2), were used for all models in Fig. 7A. The models tested were: (i) a homogeneous sphere of radius 92.6 Å (dashed line in Fig. 7A; this value compares with values of 94 Å from gel chromatography and 50–150 Å, depending on method of fixation, from electron microscopy (3)); (ii) a combination of two concentric spheres of radii 48 and 92.6 Å (ticked line in Fig. 7A); and (iii) two nonconcentric spheres with the same radii as model (ii) but with centers 20 Å apart (solid line in Fig. 7A). It may be noted that the latter two models require an interaction term, since here the amplitudes, not the intensities, are additive.

As seen in the figure, the nonconcentric two-sphere model compares more favorably with the experimental data than do the other models. However, this model does not appear to fit the experimental results as well as might be expected. To ascertain if this discrepancy is due merely to experimental error or to a small ordering

phenomenon, and to show that the particle is inhomogeneous (whether the regions are concentric or not), the distance distribution function, $p(r)$, was calculated (8) from the desmeared and unsmoothed raw data, as shown in Fig. 7B for casein submicelles at 19.38 mg/ml.

To examine the experimental distance distributions (Fig. 7B), a theoretical $p(r)$ should actually be taken as the sum of three $p(r)$ functions for spheres: one for the core region, a second for the possibly nonconcentric low electron density region, and a third for the interaction term. The $p(r)$ data of Fig. 7B were therefore fitted by an intensity function calculated for three spheres with different fractional contributions, using nonlinear regression; the resulting fit is shown as a solid line in the figure. The analysis of $p(r)$ by this method was quite satisfactory, yielding a relative standard error of 3.7%, and the results are shown in Table IV. Here D represents the diameter of a particular sphere and c represents the fraction contributed by that sphere to the total $p(r)$ distribution. As seen in the table, D_1 could represent the diameter of the loose region and D_3 the diameter of the compact region of the inhomogeneous particle.

D_2 , which represents the interaction

TABLE IV
SUM-OF-THREE-SPHERES MODEL FOR $p(r)$
(SUBMICELLES)

Fitting parameter	Value
c_1	0.773 ± 0.044
D_1 (Å)	206.3 ± 2.5
c_2	0.171 ± 0.086
D_2 (Å)	150.0 ± 10.9
c_3	0.0600 ± 0.05
D_3 (Å)	106.0 ± 11.0
RMS	0.000337

term, has a value of 150.0 ± 10.2 Å, in agreement with the theoretical 148 Å calculated from the expression $(D_1 D_3)^{1/2}$ predicted by this model. Furthermore, the D_1 and D_3 values lead to radii of gyration of 79.9 and 41.0 Å, respectively, in reasonable agreement with the values of 80.24 and 37.98 Å for R_2 and R_C in Table III. Calculation of R_2 from the $p(r)$ data in Fig. 7B up to a D_{\max} of 198.9 Å yielded a value of 78 Å, again in reasonable agreement with the value of 80.24 obtained directly from desmeared SAXS (Table III). Thus the earlier speculation that a limiting polymer, the submicelle, results from predominantly hydrophobically driven self-associations of the caseins is supported. Furthermore, the structure of this submicelle has been shown to have spherical symmetry and to consist of two different spherically shaped electron density regions, the inner, higher density region probably resulting from hydrophobic intermolecular interactions. The question of whether these two regions are exactly concentric has not been completely clarified. However, in view of Fig. 7A, the supposition that the centers are no more than approximately 20–30 Å apart is not unreasonable. The interaction term in Eq. [15] contains the function $(\sin d_{ik}h)/(d_{ik}h)$, which for small values of d_{ik} tends to unity, so that the contribution of this term is virtually constant for small center-to-center distances. The effect of the center separation on the molecular parameters can in any case not be large: since there is no destructive interference at zero angle, the parameters obtained from $i_n(0)$

(i.e., k , m , and V) remain unaffected; the effect on the radius of gyration is on the order of 5%.

Micelles. As previously reported (1, 3), addition of 10 mM calcium chloride to casein submicelles causes an aggregation of the protein to colloidal particles called casein micelles, of approximate average radii of 650 Å as determined by electron microscopy. Whether the integrity of the submicellar structure is maintained within the colloidal micelle is still a subject of much controversy (5). To address this problem, the scattering of whole casein solutions with 10 mM CaCl_2 , and no phosphate buffer to compete with the protein-calcium binding sites, was studied. The data were analyzed using a sum of three Gaussians.

The Gaussian with the largest radius of gyration was interpreted to reflect the amount of submicelles within the scattering volume ascribable to a cross section, while the other two Gaussians appear to reflect the two-electron-density spherical submicellar structure. As seen in Table II, k_2 for casein micelles was 0.308 ± 0.005 . The packing number is the inverse of this value, 3.2, representing the number of submicelles within the "cross-sectional mass" (cf. Fig. 5). It should be pointed out that the average radius of the micelles is 650 Å, as determined by electron microscopy (3); thus only cross-sectional information can be obtained from SAXS, since for a particle of this size a low enough value of the scattering angle is not experimentally accessible. What is observed is a cross-sectional portion of the colloid with molecular weight, M , of $882,000 \pm 28,000$, an electron density difference, $\Delta\rho$, of 0.0081 ± 0.0004 $e^-/\text{Å}^3$, a hydration, H , of 7.92 ± 0.42 g water/g protein (Table II) and a volume, V , of $(12.72 \pm 0.25) \times 10^6$ Å^3 (Table III). Since these results refer to cross sections only, whereas, for example, the molecular weights of whole casein micelles have been reported to range from 0.5 to 1×10^9 (16), only the hydration value can be compared with values from other studies. Our value of 7.92 is somewhat larger than the largest value reported by small-angle neutron scattering (20) of 4.0 to 5.5; that study, however, was not as detailed as this pres-

ent investigation. Other values ranging from 2 to 7 have been reported depending upon the method employed (5).

A note of caution regarding the use of the above parameters, other than the hydration, is in order. Inasmuch as they do not refer to the entire particle but only to a sample portion restricted in size by a window of scattered intensities limited by a lower small-angle limit of observation and not otherwise well defined, they cannot be used to derive any fixed relationships to the corresponding, but inaccessible, values applicable to the entire particle. Nonetheless, they are useful in affording a view of the submicellar structure, which was the aim of this investigation.

Important in this study is the comparison of molecular and structural parameters of the casein submicellar structure by itself (column one, Tables II and III) with those within the casein micelle (column two, Tables II and III). As is seen from these two tables, M_2 , k , M_C and M_L are the same, within experimental error, for the submicelles by themselves in solution and within the casein micelle. However, a substantial decrease is observed in the electron density terms $\Delta\rho_2$, and $\Delta\rho_L$, while the corresponding hydrations, volumes, and radii, H_2 , H_L , V_2 , V_L , R_2 , and R_L , increase for the submicellar particle once it is incorporated into the colloidal micelle. The V_C term increases slightly, while H_C , R_C , and $\Delta\rho_C$ for independent submicelles and for submicelles within the micellar structure are essentially the same. From the changes in these parameters it appears likely that the large swelling and hydration in the loose region is due to Ca^{2+} binding to protein electrostatic groups within this region. The relatively small changes in the density and radius of gyration of the internal core region upon the addition of calcium support the conclusion that this region consists mainly of a hydrophobically rich environment. Here again it is important to emphasize that binding of Ca^{2+} by submicelles and their subsequent incorporation into micelles does not lead to more compact structures. The electron density difference terms $\Delta\rho$ remain unaltered or decrease. Thus the low electron density ob-

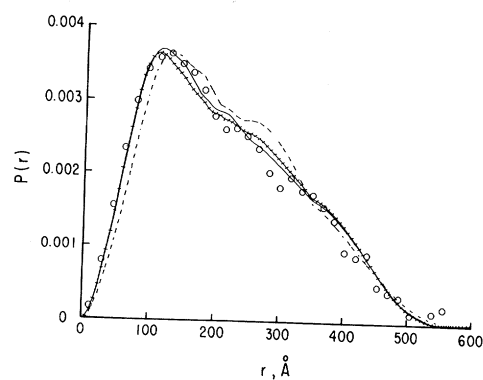


FIG. 8. Distance distribution of micelles. \circ , $p(r)$ vs r for micellar casein at 16.4 mg/ml and 10 mM CaCl_2 ; ticked line, theoretical for three inhomogeneous spheres at coordinates (0,0), (350,0), and (180,100) with same outer radii (see text); dashed line, theoretical for three inhomogeneous spheres with same outer radii in a symmetrical triangular arrangement (see text); solid line, theoretical for three inhomogeneous spheres with two different outer radii at coordinates (0,0), (350,0), and (180,0) (see Discussion). Theoretical curves were calculated by the method of Glatter (26).

served for submicelles is carried over into the structure of the micelle.

Finally, to ascertain the spatial arrangement of the three spheres within the observed "cross-sectional" scattering volume, the distance distribution function was calculated from the SAXS data for casein micelles as shown in Fig. 8. Calculation of the radius of gyration from the second moment of the $p(r)$ data in Fig. 8, to the D_{max} of 512 Å (8), yielded a value of 175.2 Å.

The experimental $p(r)$ results in Fig. 8 were then compared with theoretical curves calculated by the method of Glatter (26),⁶ using various spatial models. For these calculations the radii of the outer and inner spheres, calculated from V_2 and V_C values of column two of Table II, were 102 and 50 Å, respectively. The equilateral or symmetrical triangular arrangement gave the poorest fit to the experimental data (dashed line, Fig. 8). The Cartesian coordinates for the centers of the three inhomogeneous spheres most compatible with the experimental data were found at nonsymmetrical values of (0,0), (350,0), and (180,100) (ticked line). However, it was

found that the theoretical curve for the irregular triangular array using three inhomogeneous spheres with the same outer radius of 102 Å (ticked line) was still not as good as when the radius of the (0,0) sphere was changed to 125 Å (solid line). In fact, a value of 174.5 Å is calculated for the radius of gyration from the theoretical $p(r)$ curve for this inhomogeneous, irregular, triangular structure; this is in excellent agreement with the value of 175.2 Å found from the experimental $p(r)$ data. It will be noted that these best-fit coordinates imply interdigitation of the "loose" regions of the three submicelles (Fig. 5).

It may be concluded from these results that a discrete hydrophobically stabilized submicellar structure exists within the colloidal casein micelle, arguing against models predicting a continuous, porous gel structure, as well as those predicting an impenetrable homogeneous sphere with a "hairy surface" (5, 6). Furthermore, submicellar particles consist of an inner, spherically symmetrical, hydrophobic, and relatively electron-dense core, surrounded by a hydrophilic and less electron-dense region, both of which are substantially lower in density than are globular proteins. Upon the addition of calcium, the loose region swells with increased hydration and significantly lower electron density, which may be caused by calcium binding to hydrophilic groups within this region. Calculations of the cross-sectional scattering volume support a packing density of about 3 to 1 for the submicelles within the micelle and indicate some interaction between the loose regions of adjacent submicelles.

REFERENCES

- SCHMIDT, D. G. (1982) in *Developments in Dairy Chemistry* (Fox, P. F., Ed.), Vol. I, Applied Science, Essex, England.
- DAVIES, D. T., AND LAW, A. J. R. (1980) *J. Dairy Res.* **47**, 83-90.
- FARRELL, H. M., JR., AND THOMPSON, M. P. (1988) in *Calcium Binding Proteins* (Thompson, M. P., Ed.), Vol. II, pp. 117-137, CRC Press, Boca Raton, FL.
- PEPPER, L., AND FARRELL, H. M., JR. (1982) *J. Dairy Sci.* **65**, 2259-2266.
- WALSTRA, P. (1979) *J. Dairy Res.* **46**, 317-323.
- HOLT, C., AND DALGLEISH, D. G. (1986) *J. Colloid Interface Sci.* **114**, 513-524.
- THOMPSON, M. P. (1964) *J. Dairy Sci.* **47**, 1261-1262.
- PILZ, I., GLATTER, O., AND KRATKY, O. (1979) in *Methods in Enzymology* (Hirs, C. H. W., and Timasheff, S. N., Eds.), Vol. 61, pp. 148-249, Academic Press, San Diego.
- PESSSEN, H., KUMOSINSKI, T. F., AND TIMASHEFF, S. N. (1973) in *Methods in Enzymology* (Hirs, C. H. W., and Timasheff, S. N., Eds.), Vol. 27, pp. 151-209, Academic Press, San Diego.
- LAKE, J. A. (1967) *Acta Crystallogr.* **23**, 191-194.
- EIGEL, W. N., BUTLER, J. E., ERNSTROM, C. A., FARRELL, H. M., JR., HARWALKAR, V. R., JENNNESS, R., AND WHITNEY, R. MCL. (1984) *J. Dairy Sci.* **67**, 1599-1631.
- LUZZATTI, V., WITZ, J., AND NICOLAIEFF, A. (1961) *J. Mol. Biol.* **3**, 367-378.
- MEITES, L. (1979) *CRC Crit. Rev. Anal. Chem.* **8**, 1-53.
- GUINIER, A., AND FOURNET, G. (1955) *Small-Angle Scattering of X-Rays*, p. 128, Wiley, New York.
- KRATKY, O. (1963) in *Progress in Biophysics and Molecular Biology* (Butler, J. A. V., Huxley, H. E., and Zirkle, R. E., Eds.), pp. 123 ff, Pergamon-MacMillan, New York.
- SCHMIDT, D. G., AND PAYENS, T. A. J. (1976) in *Surface and Colloid Science* (Matijevic, E., Ed.), pp. 165-229, Wiley, New York.
- LUMRY, R., AND ROSENBERG, A. (1975) *Colloq. Int. CNRS* **246**, 53-62.
- RICHARDS, F. M. (1974) *J. Mol. Biol.* **82**, 1-14.
- LUZZATTI, V., WITZ, J., AND NICOLAIEFF, A. (1961) *J. Mol. Biol.* **3**, 379-392.
- STOTHART, P. H., AND CEBULA, D. J. (1982) *J. Mol. Biol.* **160**, 391-395.
- TANFORD, C. (1961) *Physical Chemistry of Macromolecules*, p. 236, Wiley, New York.
- KUNTZ, I. D., AND KAUZMANN, W. (1974) *Adv. Protein Chem.* **28**, 239-345.
- PESSSEN, H., KUMOSINSKI, T. F., AND FARRELL, H. M., JR. (1988) *J. Ind. Microbiol.* **3**, 89-103.
- BERNSTEIN, F. C., KOETZLE, T. F., WILLIAMS, G. J. B., MEYER, E. F., JR., BRICE, M. D., RODGERS, J. R., KENNARD, O., SHIMANOUCI, T., AND TASUMI, M. (1977) *J. Mol. Biol.* **112**, 535-542.
- DEBYE, P. (1915) *Ann. Physik.* **46**, 809-823.
- GLATTER, O. (1980) *Acta Phys. Austriaca* **52**, 243-256.